AD_____

GRANT NO: DAMD17-94-J-4424

TITLE: Single-pulse dual-energy mammography using a binary screen coupled to dual CCD cameras.

PRINCIPAL INVESTIGATOR: John M. Boone, Ph.D.

CONTRACTING ORGANIZATION:
The Regents of the University of California
Office of Research
410 Mrak Hall
University of California, Davis
Davis, CA 95616-8671

REPORT DATE: August 4, 1995

TYPE OF REPORT: Annual Report

PREPARED FOR: U.S. Army Medical Research and
Materiel Command
Fort Detrick, Maryland 21702-5012

DISTRIBUTION STATEMENT: Approved for public release
distribution unlimited

REPORT DOCUMENTATION PAGE

Form Approved
OMB No. 0704-0188

1. AGENCY USE ONLY (Leave blank)	2. REPORT DATE	3. REPORT TYPE AND DATES COVERED
	August 4, 1995	Annual 15 Jul 94 - 14 Jul 95

4. TITLE AND SUBTITLE
Single-Pulse Dual-Energy Mammography Using a Binary Screen Coupled to Dual CCD Cameras

5. FUNDING NUMBERS
DAMD17-94-J-4424

6. AUTHOR(S)
Dr. John M.Boone

7. PERFORMING ORGANIZATION NAME(S) AND ADDRESS(ES)
University of California, Davis
Davis, California 95616-8671

8. PERFORMING ORGANIZATION REPORT NUMBER

9. SPONSORING / MONITORING AGENCY NAME(S) AND ADDRESS(ES)
U.S. Army Medical Research and Materiel Command
Fort Detrick, Maryland 21702-5012

10. SPONSORING / MONITORING AGENCY REPORT NUMBER

11. SUPPLEMENTARY NOTES

12a. DISTRIBUTION / AVAILABILITY STATEMENT
Approved for public release, distribution unlimited

12b. DISTRIBUTION CODE

13. ABSTRACT *(Maximum 200 words)*

Normal progress on the scientific objectives of this project are reported. The post-doc has been hired, and is now up to speed with the project. Monte Carlo calculations have been run over an extended period of time, and the scattered photon distribution is now well characterized for clinically relevant breast thicknesses (3-8 cm) and x-ray energies (10-60 keV). In order to characterize different breast parenchyma patterns, a computer score called the Breast Density Index has been conceived and tested, comparing it with the density scoring of an experience mammographer. The design of the dual energy mammography system has been refined, and the mechanical framework for the system is currently being fabricated at a machine shop. A new technique for easily determining the MTF of the optics and CCD camera is being evaluated with promising results. DQE measurements are also underway. The Deslattes x-ray spectrometer is being used in the laboratory to catalog measured x-ray spectra from our mammography system. This device also promises to be very useful in measuring the attenuation coefficients of tissue specimens.

14. SUBJECT TERMS
Dual Energy, Mammography, Digital Imaging, Calcification

15. NUMBER OF PAGES
27

16. PRICE CODE

17. SECURITY CLASSIFICATION OF REPORT	18. SECURITY CLASSIFICATION OF THIS PAGE	19. SECURITY CLASSIFICATION OF ABSTRACT	20. LIMITATION OF ABSTRACT
Unclassified	Unclassified	Unclassified	Unlimited

GENERAL INSTRUCTIONS FOR COMPLETING SF 298

The Report Documentation Page (RDP) is used in announcing and cataloging reports. It is important that this information be consistent with the rest of the report, particularly the cover and title page. Instructions for filling in each block of the form follow. It is important to *stay within the lines* to meet *optical scanning requirements*.

Block 1. Agency Use Only *(Leave blank)*.

Block 2. Report Date. Full publication date including day, month, and year, if available (e.g. 1 Jan 88). Must cite at least the year.

Block 3. Type of Report and Dates Covered. State whether report is interim, final, etc. If applicable, enter inclusive report dates (e.g. 10 Jun 87 - 30 Jun 88).

Block 4. Title and Subtitle. A title is taken from the part of the report that provides the most meaningful and complete information. When a report is prepared in more than one volume, repeat the primary title, add volume number, and include subtitle for the specific volume. On classified documents enter the title classification in parentheses.

Block 5. Funding Numbers. To include contract and grant numbers; may include program element number(s), project number(s), task number(s), and work unit number(s). Use the following labels:

C	- Contract	**PR**	- Project
G	- Grant	**TA**	- Task
PE	- Program Element	**WU**	- Work Unit Accession No.

Block 6. Author(s). Name(s) of person(s) responsible for writing the report, performing the research, or credited with the content of the report. If editor or compiler, this should follow the name(s).

Block 7. Performing Organization Name(s) and Address(es). Self-explanatory.

Block 8. Performing Organization Report Number. Enter the unique alphanumeric report number(s) assigned by the organization performing the report.

Block 9. Sponsoring/Monitoring Agency Name(s) and Address(es). Self-explanatory.

Block 10. Sponsoring/Monitoring Agency Report Number. *(If known)*

Block 11. Supplementary Notes. Enter information not included elsewhere such as: Prepared in cooperation with...; Trans. of...; To be published in.... When a report is revised, include a statement whether the new report supersedes or supplements the older report.

Block 12a. Distribution/Availability Statement. Denotes public availability or limitations. Cite any availability to the public. Enter additional limitations or special markings in all capitals (e.g. NOFORN, REL, ITAR).

DOD	- See DoDD 5230.24, "Distribution Statements on Technical Documents."
DOE	- See authorities.
NASA	- See Handbook NHB 2200.2.
NTIS	- Leave blank.

Block 12b. Distribution Code.

DOD	- Leave blank.
DOE	- Enter DOE distribution categories from the Standard Distribution for Unclassified Scientific and Technical Reports.
NASA	- Leave blank.
NTIS	- Leave blank.

Block 13. Abstract. Include a brief *(Maximum 200 words)* factual summary of the most significant information contained in the report.

Block 14. Subject Terms. Keywords or phrases identifying major subjects in the report.

Block 15. Number of Pages. Enter the total number of pages.

Block 16. Price Code. Enter appropriate price code *(NTIS only)*.

Blocks 17. - 19. Security Classifications. Self-explanatory. Enter U.S. Security Classification in accordance with U.S. Security Regulations (i.e., UNCLASSIFIED). If form contains classified information, stamp classification on the top and bottom of the page.

Block 20. Limitation of Abstract. This block must be completed to assign a limitation to the abstract. Enter either UL (unlimited) or SAR (same as report). An entry in this block is necessary if the abstract is to be limited. If blank, the abstract is assumed to be unlimited.

*U.S.GPO:1993-0-358-779

FOREWORD

Opinions, interpretations, conclusions and recommendations are those of the author and are not necessarily endorsed by the US Army.

JWB Where copyrighted material is quoted, permission has been obtained to use such material.

____ Where material from documents designated for limited distribution is quoted, permission has been obtained to use the material.

JWB Citations of commercial organizations and trade names in this report do not constitute an official Department of Army endorsement or approval of the products or services of these organizations.

____ In conducting research using animals, the investigator(s) adhered to the "Guide for the Care and Use of Laboratory Animals," prepared by the Committee on Care and Use of Laboratory Animals of the Institute of Laboratory Resources, National Research Council (NIH Publication No. 86-23, Revised 1985).

____ For the protection of human subjects, the investigator(s) adhered to policies of applicable Federal Law 45 CFR 46.

____ In conducting research utilizing recombinant DNA technology, the investigator(s) adhered to current guidelines promulgated by the National Institutes of Health.

____ In the conduct of research utilizing recombinant DNA, the investigator(s) adhered to the NIH Guidelines for Research Involving Recombinant DNA Molecules.

____ In the conduct of research involving hazardous organisms, the investigator(s) adhered to the CDC-NIH Guide for Biosafety in Microbiological and Biomedical Laboratories.

Accession For	
NTIS GRA&I	☑
DTIC TAB	☐
Unannounced	☐
Justification	
By	
Distribution/	
Availability Codes	
Dist	Avail and/or Special
A-1	

PI Signature

August 4, 1995
Date

Table of Contents

1. Introduction

1.1 Nature of the Problem

This project involves the design, construction, and testing of a novel digital mammography system. The basic approach to acquiring the image data using CCD camera technology is similar to the work of others. However, the proposed system incorporates a *binary* screen as the primary x-ray receptor. A binary screen is an intensifying screen composed of two different phosphors mixed into the screen. Phosphor 1 has a low k-edge (e.g. Y_2O_2S, k-edge$_Y$ = 17 keV), and therefore will preferentially absorb the lower energy x-ray photons in the spectrum incident upon the detector. Phosphor 1 emits light of a specific wavelength, and because rare earth phosphors emit in a relatively narrow optical range, it is straightforward to optically isolate the wavelengths emitted by phosphor 1 with a CCD camera 1 focused onto the binary screen. Phosphor 2 has a higher energy k-edge (e.g. Gd_2O_2S, k-edge$_{Gd}$ = 50 keV), and therefore will preferentially absorb the higher energy x-ray photons incident upon the detector. As with Phosphor 1, Phosphor 2 has its own characteristic wavelength emission and a CCD camera 2 is tuned to only detect the light emission from Phosphor 2. The system is illustrated in Figure 1.

The two-camera setup can acquire two different images simultaneously, one corresponding to mostly low energy x-ray photons, the other to mostly high energy photons. From the low energy image, $I_L(x,y)$ and the high energy image, $I_H(x,y)$, the dual-energy subtracted image, $S(x,y)$, can be calculated as:

$$S(x,y) = LN[\, I_L(x,y)\,] - R\, LN[\, I_H(x,y)\,]$$

R is a constant that determines the type of material that is subtracted, either calcium, fat, or some intermediate material (glandular tissue). Dual energy subtraction is well known and a detailed discussion will therefore be avoided.

1.2 Background

Breast cancer will strike approximately one in nine women in the United States, making it the most common form of cancer amongst women. In 1992, there were over 46,000 deaths due to breast cancer and 180,000 new cases were detected. Presently, there is no cure for this devastating disease and the best hope for patients stricken with breast cancer lay in its early detection. While ultrasound and MRI are modalities that have been aimed at the breast, x-ray mammography has the best sensitivity for the early detection of breast cancer in women who are asymptomatic. Hence, screen film mammography has proliferated substantially over the last 5 years as an important "front line" against breast cancer.

Digital radiography has been investigated by many researchers with many different motives. Digital mammography pushes digital acquisition techniques to their technical limits due to the high spatial resolution and low dose requirements imposed by breast imaging. One generic

advantage of digital radiography is that the detector technology is divorced from the display technology, unlike in screen-film systems. By divorcing detection and display, each of those responsibilities can be assigned to dedicated equipment, and therefore the detector can be optimized for detection, and the display device can be optimized for display. Electronic detectors also have significantly better dynamic range than conventional screen-film combinations. The whole breast can be imaged without loss of contrast in regions of too low or too high exposure, as often occurs with screen-film systems. Another excellent example where digital detectors may play an important role in cancer detection is with dual-energy mammographic acquisition. In dual-energy imaging, calcified areas of the patient can be enhanced due to the intrinsic physical properties of x-ray absorption, as opposed to pattern recognition or imaging processing enhancements. Since the breast contains no naturally occurring calcific structures (i.e. no bones) and since calcification is a very important diagnostic finding in the diagnosis of breast cancer, dual-energy imaging has great potential in mammography. Dual-energy acquisition requires the detection of two images, one at low x-ray energies and the other at a higher energies. The first phase of this project is to build digital mammographic acquisition hardware and the software necessary to control digital acquisition. The second phase is to demonstrate using phantoms, tissue specimens, and a few pre-selected patients, the feasibility of dual energy mammography in the screening mammography setting.

1.3 Previous Studies

The image intensifier has been used as the primary detector for one system[1], coupled with a scanning slit arrangement which collimates the x-ray beam down to a thin slit. In this system, the image is formed by capturing the light output of the image intensifier using a linear 4k charge coupled device (CCD). While the spatial resolution of the 4k linear detector was superb, there was a 20% increase in x-ray dose due to the penumbra cast by the fore-slit (i.e. some of the primary beam didn't contribute to image formation) In addition, the image intensifier is difficult to modify given its complexity and vacuum environment, and the detection efficiency of the CsI input phosphor used in commercially available image intensifiers cannot be easily optimized in the low x-ray energy region typically used in mammography.

Photostimulable phosphor systems (PSPs) have achieved good market success for general radiology, and this technology is the cornerstone of present day "digital radiography" (as opposed to digital mammography). It is known that the commercial manufacturers of PSP systems are trying to develop high resolution systems for mammography, and several research groups have also reported using photostimulable phosphors for mammography. Nevertheless, this approach will require significant further refinements to ever meet the demands of clinical radiologists involved in mammography.

Karellas[2] has reported on the use of a CCD camera optically focused on an intensifying screen for use in digital mammographic imaging. This article contains a good description of the use of optically-coupled CCDs, and includes an analysis of the limitations of the technique as well. The authors report that an optical coupling efficiency of 0.0082 was achieved with a field of view of 90 mm x 90 mm and an *f*/1.2 lens. The authors continue to point out that, "... an even greater optical efficiency may be required in order to achieve a level well above a secondary quantum sink." For realistic clinical mammography, a field of view on the order of 200 mm x 200 mm is necessary to accommodate most breasts. As the field of view gets larger, the

demagnification factor gets larger, and the optical coupling efficiency is reduced dramatically due to solid angle effects. Per Karellas[2]:

$$\eta = T / [1 + 4f^2(m+1)^2]$$

where η is the light capture efficiency, T is the bulk transmission factor (typically around 0.8), f is the f-number of the lens and m is the demagnification factor. Using this equation, the light coupling efficiency for a very fast lens (*f*/0.7), a 200 mm x 200 mm field of view and a 25.4 mm x 25.4 mm CCD chip would be 0.0051. This means that approximately one out of every 200 light photons emitted from the screen would strike the CCD chip. The number of light photons emitted from an intensifying screen per absorbed photon is highly dependent on screen characteristics, and this number has been reported to be as high as 400 to 600 photons per x-ray interaction[3]. Using a value of 500, this would mean that only 2.5 optical photons would strike the CCD chip per absorbed x-ray in the intensifying screen. With a conversion efficiency of the CCD of about 0.5 electrons/optical photon, the 2.5 optical photons would yield 1.25 electrons. Given the fairly broad statistical distribution of these conversion events[4,5], a 1.25 *mean* electron yield per absorbed x-ray photon would result in significant quantum noise due to the optical coupling stage in the detector. Mickish and Beutel[3] have described the optical photon yield per x-ray photon. From their work, a Gd_2O_2S screen emits on the order of 500 photons per 22 keV x-ray.

Of course other considerations such as detector amplifier noise haven't been considered above. Also, a fast lens such as an *f*/0.7 has a very limited depth of field, and consequently one would expect the resolution in the periphery of the image to be reduced as a result.

Herron has coupled a 116 mm diameter screen with a 2k x 2k CCD detector using a fiber optic minifier with a proximity-focused intensifier tube placed between the fiber optic minifier and the CCD chip. The intensifier tube had 50 line pair/mm resolution, and provided gains from 5 to 30 in the system. The system achieved fair resolution with the 10% MTF value falling at approximately 4 lp/mm. Although a 116 mm circular field of view is much smaller than the necessary 200 mm x 200 mm *square* field of view required to image a majority of women, the performance of this system is encouraging.

The PI and Dr. Tecotzky (who is the original developer of rare-earth phosphors for radiological imaging, and is a paid consultant on this proposal) have worked on detector optimization problems using computer simulations in previous investigations[6,7,8]. Any (x-ray quantum limited) detector system can deliver a better signal to noise ratio (SNR) by simply increasing the incident x-ray flux, but this of course has an impact in terms of increased dose to the patient. Therefore, optimization of detector design must include the consequences of dose to the patient. One convenient measure that folds both detector performance and patient dose into the same equation is the figure of merit (FOM) defined as:

$$FOM = (\text{Contrast} \cdot SNR)^2 / \text{Glandular Dose}$$

Because the SNR is related to the incident x-ray exposure by $N^{1/2}$, and the glandular dose is proportional to N, the above quantity is independent of the exposure levels used in imaging. This eliminates this parameter from the optimization procedure. We have used this figure of merit in the past[6,7,8,9]. For example, to optimize the performance of a dual-phosphor binary

screen detector with respect to the kV of the spectrum and the pre-patient filtration, the FOM was computed as a function of the atomic number (Z) of the pre-patient filter and of the kV. The binary screen is a screen designed with two homogeneously mixed phosphors, each with different k-edges, and each emits a different color of light. The binary screen design permits single-pulse dual-energy acquisition using two CCD cameras. The optimization results for a 10 cm tissue equivalent patient are seen below:

Scattered radiation is an important contribution to the dose term in this FOM, and also has a significant impact on the contrast. To use this FOM in the simulation environment, therefore, a full understanding of the distribution of scattered radiation dose deposition is important to the accurate assessment of glandular dose. The PI and Dr. Seibert (co-investigator) have employed Monte Carlo simulation as a means of studying the distribution of scattered x-ray energy both to the detector and to the patient. Recently, the PI has reported on the parameterization of the dose due to primary and scatter in tissue as a function of incident x-ray energy and tissue thickness[9], specifically to make detector optimization studies easier.

2. Body of Report

The initial progress of this research is proceeding well. There were a large number of somewhat perfunctory but nevertheless time consuming tasks that were accomplished this past year. The post-doc has been hired, and Dr. Tong Yu is now up to speed with the project and making excellent progress. The principal investigator has met several times with each of the consultants, one a mechanical engineer (Roger Malcolm, M.S.E) and the other a rare earth phosphor chemist (Mel Tecotzky, Ph.D.). In each instance, these consultative sessions have resulted in new ideas with respect to design of the digital mammography system. Furthermore, the physical construction of the digital mammography system is underway, with crucial elements currently being fabricated by the machine shop under control of the mechanical engineer consultant, Roger Malcolm. Phosphors have also been received by the rare earth chemist for testing in a new detector system.

Monte Carlo code specifically for the evaluation of scatter in the mammography x-ray energies has been written (modified from previous code written entirely by the PI) and was run for approximately 3 months, acquiring scatter distribution data necessary for calculating its effect both on glandular dose and on the contrast and SNR in the image.

Ordering and receiving materiel at the University of California can in some instances require 6 or more months. We have anticipated this "lead time" and have ordered many of the items crucial to the development of the dual energy digital mammography system.

For completeness, we include below the tasks identified in the ***statement of work*** for the first year of this four year project. As shown below on the timeline given in the grant,

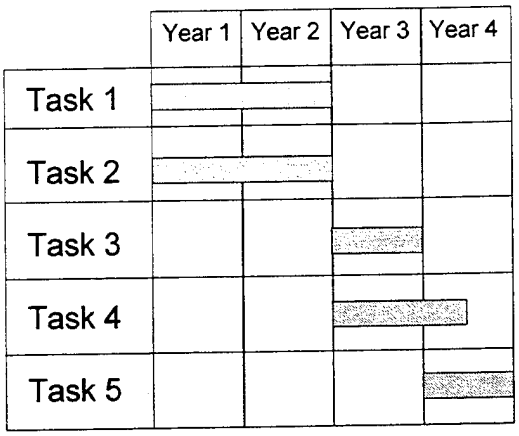

Tasks 1 and 2 are each two year tasks and therefore both sub-projects are still in progress. We list each of the tasks as stated in the grant ("Statement of Work") and identify our progress to date:

Task 1: Computer Simulation of Dual-Energy Digital Mammography System [months 1-24]

1.1. The most efficient x-ray spectrum, which depends on the anode target material (Molybdenum or Tungsten), the kilovoltage, and the thickness and composition of the pre-patient filter, will be identified for dual energy mammography
1.2. The most efficient x-ray spectrum, which depends on the anode target material (Molybdenum or Tungsten), the kilovoltage, and the thickness and composition of the pre-patient filter, will be identified for single energy mammography
1.3. The best thickness and phosphor ratio (e.g. mg Y_2O_2S versus mg Gd_2O_2S) for dual energy mammography will be identified using computer simulation with a typical breast thickness (4.2 cm).
1.4. The most efficient anti-scatter grid ratio and construction will be identified using the figure of merit [Contrast x SNR]^2 / [Average Glandular Dose]

2.1 Computer Simulation Studies

We are exploring in the simulation environment modifications to the acquisition geometry from the binary screen system laid out in Figure 1. The modified geometry is shown in Figure 2. The modified geometry has the potential of increasing the energy separation between the low and high energy images, and therefore improving the image quality in the final, dual energy subtracted image. In addition to the slight change in mechanical geometry, we have also thought of a new and potentially better way of acquiring the image in the temporal domain. The technique is demonstrated graphically in Figure 3. The fact that the CCD cameras for the high and the low energy images can be triggered independently allows gated acquisition, where the "on" and "off" gate controls over the time course of the scan can be controlled separately for the low and the high energy images (CCD cameras). In addition, the kV can be rapidly switched *during* the acquisition, still using a single pulse. This idea was inspired in part by the work of Dr. Robert Alverez, who has been studying using this temporal gating to achieve improved SNR in dual energy radiography using stacked photostimulable phosphor plates[10]. His idea is to erase

the image on the front (low energy) imaging plate during the high energy acquisition, using a strong light which will erase the latent image on the low energy PSP imaging plate. Of course with the electronic cameras in our application, erasure is not necessary because each of the CCD cameras can be gated independently. Dr. Alvarez has demonstrated an approximately 10 fold improvement[10] in the SNR using his technique, and because of the more precise nature of electronic gating in our application in addition to the better selection of x-ray phosphors available, we are optimistic that similar or better improvements can be achieved in our laboratory.

The Monte Carlo code was modified for this mammography application and ran alone for three months on our DEC 3000 workstation. Thus for glandular tissue, we have relatively noiseless data concerning the distribution of x-ray photons, characterized both as functions of input x-ray energy and breast thickness. Examples of these distributions are shown in Figures 4, 5 and 6. We have made similar characterizations for all permutations including 3, 4, 5, 6, 7 and 8 cm of breast tissue against input x-ray photon energies of 10 to 60 keV (by 1 keV intervals). The monoenergetic data calculated can be combined with known x-ray spectra to properly simulate the realistic situation during dual energy imaging.

Tasks 1.1 and 1.2 involve the use of x-ray spectra. Although it was originally envisioned that tabular x-ray spectra would be used, since the award was made we have been collaborating with Dr. Richard Deslattes at NIST, who received a US Army grant (M4539FU6, "Crystal diffraction spectrometry for accurate, non-invasive kV/spectral measurement for improvement of mammographic image quality"). We just received one of the first x-ray spectrographs from Dr. Deslattes and are currently designing a study to completely measure and document a wide assortment of clinical mammography x-ray spectra. This study is consistent with our goal of verifying the correspondence between Monte Carlo studies and between experimentally measured quantities. Such a verification process has been confounded in the past by imprecise correspondence between the measured and modeled x-ray spectra. With the x-ray spectrograph now in hand, we can make comparisons between experimental measurements and Monte Carlo calculations with a sound knowledge of the spectra. As an example of the utility of the Deslattes spectrometer, Figure 7 shows two spectra measured with this device on our laboratory mammography machine (Senograph 500T). The two spectra differ by the addition of 1.0 mm of aluminum. Not only are the spectra themselves useful in their own right, the excellent energy resolution of the spectrometer (compared to photon counting approaches) allows the measurement of energy dependent attenuation coefficients of a wide assortment of materials. An illustrative example of this is shown in Figure 8, where the two spectra shown in Figure 7 were used to calculate the mass attenuation coefficient for a 1.0 mm sheet of aluminum. The measured data is compared against the tabulated[11] attenuation coefficients, and reasonably good correspondence is shown in these preliminary data. We intent to obtain thin sections of various types of breast tissues (fat, glandular), and make detailed and accurate determinations of the attenuation coefficients of this materials. Although this has been done before[12], the energy resolution of the Deslattes spectrometer is much greater than pulse-height spectrometry and therefore we consider this an important undertaking.

We are also currently installing a dedicated angiography system (A Toshiba, 2000 mA constant potential generator) in our x-ray laboratory. This system is an update to an older (1966) x-ray system that was recently decommissioned. Because our previous study on dual energy radiography{23} showed, using hypothetical monoenergetic spectra, that a 74 keV beam was most efficient for the high energy beam (with Y_2O_2S/Gd_2O_2S detector pairs), it will be necessary

to use the newly installed tungsten anode system for verification of the dual energy optimization studies.

Tasks 1.3 and 1.4 are computer simulations and calculations that result from the data collected in tasks 1.1 and 1.2. Once the spectral measurements are finished and tasks 1.1 and 1.2 are completed, it is relatively straightforward to proceed with tasks 1.3 and 1.4. With respect to task 1.4, we have purchased a variety (12:1, 10:1, 8:1, and 5:1) of antiscatter grids in order to make experimental verifications with Monte Carlo results.

Task 2: Design and Construct Dual-Energy Mammography Imaging System [months 1-24]

2.1. Consult with mechanical engineer (consultant on project) and finalize design for the mechanical construction of the system housing, and have EOT, Inc build it.
2.2. Purchase optical supports and cameras, and mount them inside the completed housing (2.A). Interface optical and electronic components to microcomputer, and microcomputer to x-ray generator. Write software to orchestrate both auto-calibration procedures as well as digital image acquisition.

2.2 Mechanical Construction (and evaluation) of Dual Energy System

We have begun the detailed scientific evaluation of the CCD cameras that are presently in our laboratory, including the determinations of MTF(f) and DQE(f). Developing the techniques and the necessary computer code for making these measurements will be useful for when the full resolution CCD cameras, which we are now in the process of ordering, arrive. We found a company that manufactures optical sine wave phantoms, and have purchased one. Such a phantom allows the direct calculation of MTF from the measured sine wave image, by computed the modulation at a frequency f as:

$$\text{Modulation}(f) = (\text{MAX}-\text{MIN}) / (\text{MAX}+\text{MIN})$$

By normalizing the modulation to the f=0 value, a modulation transfer function (MTF) of the camera and the optics can be easily determined. We are presently evaluating this technique, with a manuscript in preparation. The sine wave test pattern results are compared with the more conventional Fourier Transform of a line spread function approach, in Figure 9.

In order to determine the quantum detection efficiency (QDE(f)) of a CCD camera-lens system, it is necessary to know the number of quanta incident upon the system. We are presently making these measurements, and a manuscript is in preparation which will report the DQE(f) of CCD cameras-lens systems for a variety of different parameters such as demagnification factor, wavelength of the light (545 nm and 624 nm) and lens f-stop. An example of such a DQE(f) measurement is shown in Figure 10.

Because of these new developments in terms of design permutations, we recognized the importance of having a flexible mechanical system for experimental measurements and verification. Consequently, we have devoted a great deal of time in designing the mechanical layout of the dual energy mammography system. Instead of using an inflexible box to mount the system in, which was the original design, we have gone to a much more flexible design of the mammography system in consultation with Roger Malcolm, our consultant on mechanical design.

The mechanical configuration of the dual energy mammography system is illustrated schematically in Figure 2. The hardware necessary for building the physical system, including camera, detector, and mirror mounts, are currently being fabricated and we expect receipt of the remaining necessary items within a few weeks. We have chosen to design the mechanical aspects of the system so that significant modification can be made, reflecting our newer thoughts on optimizing the SNR in the dual energy subtracted image. The system modular construction design using a three dimensional optical rail system is shown in Figure 11. This rail system essentially extends the 2 dimensional optical table to the third dimension, and will act as the mechanical framework for the dual energy mammography system. Optical pathways will be kept light-tight using camera bellows, which have recently been ordered. The 1" square cross section aluminum struts have clear holes drilled (for 1/4-20 screws to pass through), and we have ordered the custom fabrication of quantities of struts in lengths from 1.0 foot to 8.0 feet. An enlargement of the struts is illustrated in Figure 12, and a rotating connection collar (flange) for coupling the linear struts is shown in Figure 13. This rotating flange will allow complete flexibility in positioning the various elements of the digital mammography system, including the compression device, breast support, cameras, mirrors, and screens.

3. Conclusions

Progress has been made in this first year of the project. The post-doc has been hired, is settled in and has a solid focus on this project. Much of the equipment necessary for building the dual energy mammography system has been ordered, for example the optical benches, micropositioning equipment, lasers for alignment, stepping motors and their supporting electronics, a computer and display, etc. The design of the mechanical aspects of the system is close to complete, and the necessary hardware is being custom fabricated by a high tech machine shop. Monte Carlo simulations have been run with a large number of virtual photons in order to reduce the quantum noise in the subsequent calculations.

There are many aspects to this project, and in this first year in order to "ramp up" as fast as possible, we have pursued many of the development issues in parallel. The first two tasks, as identified in the ***statement of work***, are well underway with preliminary results. The parallel approach has got us started on, and well into, many of the important sub-projects, however it leaves us at this one year mark with several tasks in progress. This is how the project was laid out in the original proposal.

Several innovations and improvements over the original design have been developed. The different layout of the dual energy system should yield better quality images due to increased energy separation between the low and the high energy images. The newly proposed sequence for image acquisition (Figure 3), involving pulsed x-ray switching and independently gated, dual camera acquisition should also yield superior dual energy image quality. The availability of the Deslattes spectrometer will allow us to more accurately assess mammography x-ray spectra, and will in turn allow for a more precise verification of the Monte Carlo simulations.

In summary, we are more excited about the prospects of dual energy digital mammography than we were last year. Progress towards the development and construction of the system is going as planned.

4. References

1. M. Yaffe, R. Nishikawa, A. Maidment, and A. Fenster, "Development of a digital mammography system," SPIE.**914,** 182 (1988)
2. A. Karellas, L.J. Harris, H. Liu, M.A. Davis, and C.J. D'Orsi, "Charge-coupled device detector: performance considerations and potential for small-field mammographic imaging applications," Med. Phys.**19,** 1015-1023 (1992)
3. D. Mickish and J. Beutel, "The determination of x-ray phosphor scintillation spectra," SPIE.**1231,** 327 (1990)
4. G.T. Barnes, "Radiographic mottle: A comprehensive theory," Med. Phys.**9,** 656-667 (1982)
5. R.M. Nishikawa and M.J. Yaffe, "Model of the spatial-frequency dependent detective quantum efficiency of phosphor screens," Med. Phys.**17,** 894-904 (1990)
6. J.M. Boone, G.S. Shaber, and M. Tecotzky, "Dual-energy mammography: a detector analysis," Med. Phys.**17,** 665-675 (1990)
7. J.M. Boone, M. Tecotzky, and G.M. Alexander, "Binary screen detector system for single-pulse dual-energy radiography," Radiology.**183,** 863-870 (1992)
8. J.M. Boone and J.A. Seibert, "A comparison of mono- and poly-energetic x-ray beam performance for radiographic and fluoroscopic imaging," Med. Phys.**21,** 1853-1863 (1994)
9. J.M. Boone, "Parametrized x-ray absorption in diagnostic radiology from Monte Carlo calculations: implications for x-ray detector design," Med. Phys.**19,** 1467-1473 (1992)
10. R.E. Alvarez, "Active energy selective detector for dual energy computed radiography (abstract)," Radiology.**189(P),** 129 (1995)
11. M.H. McMaster, N.K. Del Grande, J.M. Mallett, and J.M. Hubbell, "Compilation of x-ray cross sections," U.S. Dept of Commerce. Springfield, VA. (1969)
12. P. Johns, D. Drost, M. Yaffe, and A. Fenster, "Dual energy mammography: initial experimental results," Med. Phys.**12,** 297 (1985)

5. Appendix

Figure Number	Description
Figure 1	A diagram showing the configuration of the dual energy mammography system as originally proposed.
Figure 2	A diagram showing the configuration of the dual energy mammography system modified for a sandwiched detector.
Figure 3	The timing sequence used to acquire dual energy mammograms using two CCD cameras in the configuration shown in Figure 2.
Figure 4	Monte Carlo simulation results, 3 cm breast and 15 keV incident x-ray photon
Figure 5	Monte Carlo simulation results, 5 cm breast and 25 keV incident x-ray photon
Figure 6	Monte Carlo simulation results, 8 cm breast and 55 keV incident x-ray photon
Figure 7	Two x-ray spectra measured in our laboratory using the Deslattes x-ray spectrometer.
Figure 8	An example of how the attenuation coefficients for various tissue types can be (easily) evaluated using the Deslattes x-ray spectrometer. The measured versus theoretical mass attenuation coefficients for aluminum are shown.
Figure 9	9A illustrates the influence of an imaging system on modulation of a sine wave input. 9B illustrates MTF measurements taken both conventionally (by Fourier transform of the line spread function) and using the sine wave test pattern.
Figure 10	The noise power spectrum for the optical/CCD imaging system presently in our laboratory.
Figure 11	An engineering drawing of the modular design of the mechanical support for the digital mammography system
Figure 12	A blow up drawing of the struts.
Figure 13	A blow up drawing of the rotating flange assembly used for connecting the struts together.

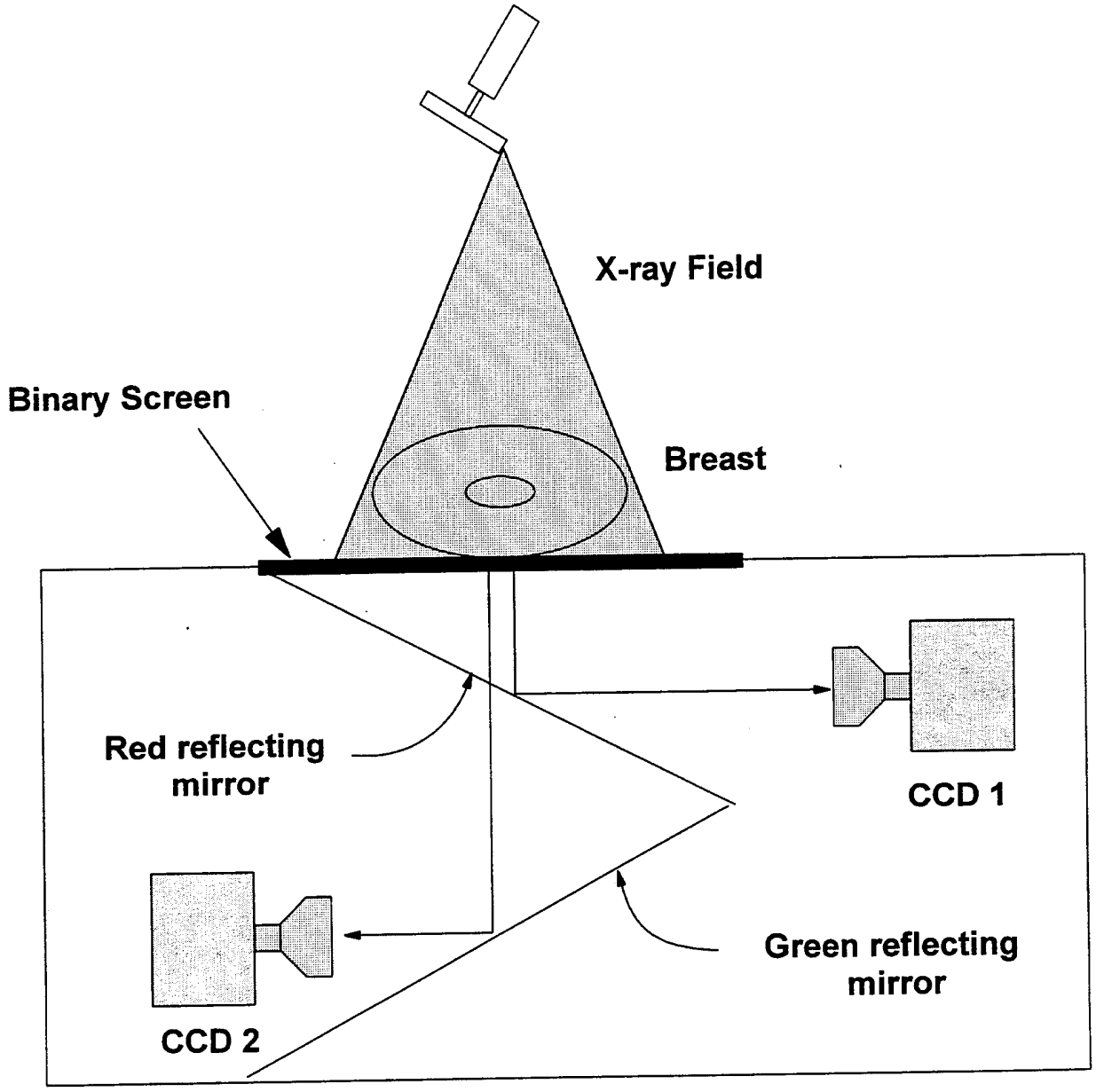

Figure 1: The binary screen is composed of two x-ray phosphors, for example Y2O2S:Eu (624 nm-red emitting) and GdO2S:Tb (545 nm-green emitting). The Yttrium phosphor preferentially absorbs low energy x-rays, and the Gadolinium phoshor preferentially absorbs the high energy x-rays, due to their respective k-edges. By filtering the light that enters each of the CCD cameras using dichroic mirrors, the low energy x-ray signal can be isolated in CCD 1 and the high energy signal can be isolated in CCD 2.

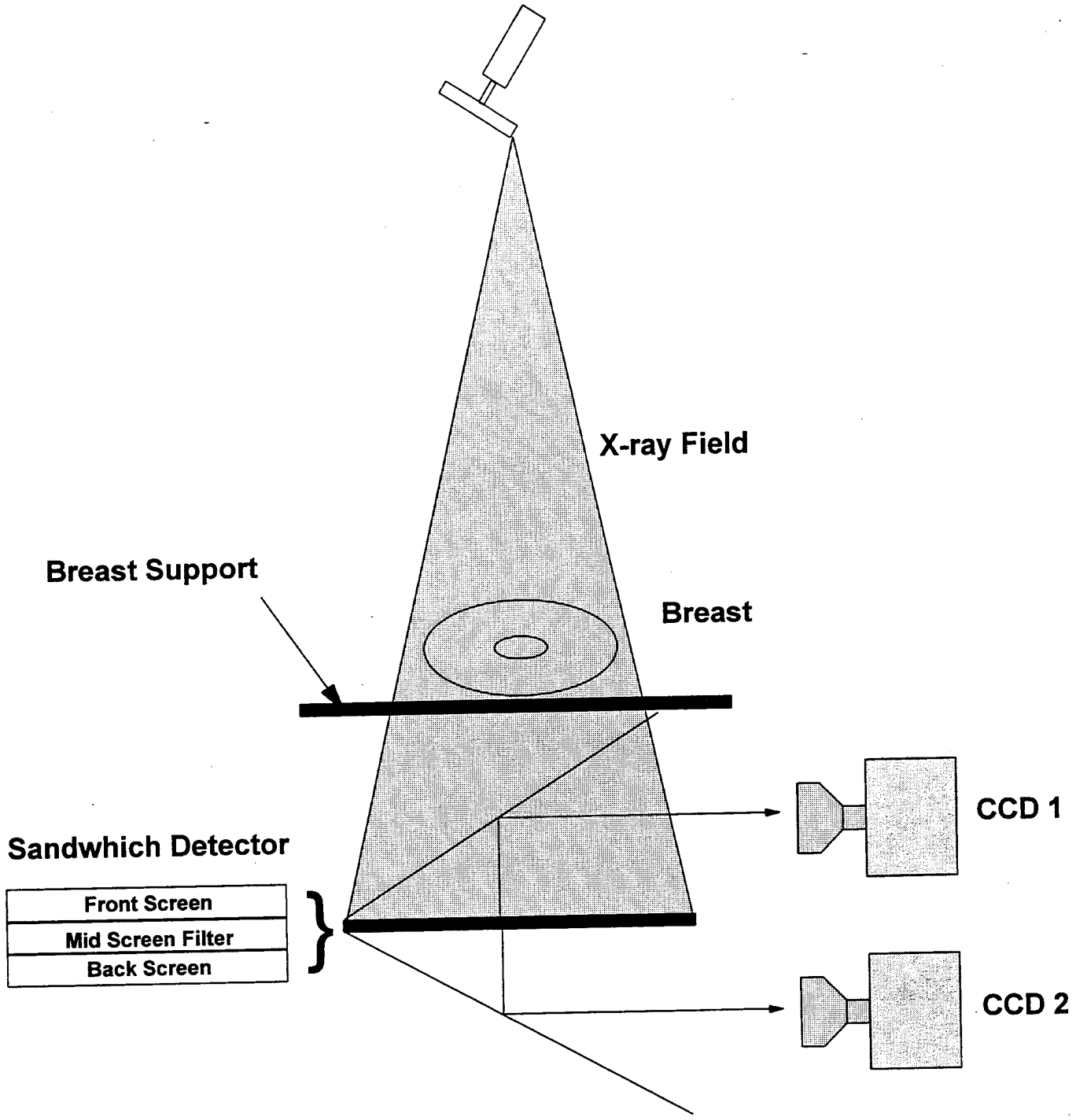

Figure 2: Modified geometry for dual energy mammography system. This approach makes use of a sandwhich detector, familiar to dual energy researchers in the photostimulable phosphor arena. CCD 1 records the image from the front, low energy phosphor, and CCD 2 records the image from the back, high energy phosphor. Although this geometry is similar conceptually to sandwhiched PSP detectors, here we have substantially more flexibility in terms of phosphor selection. In addition, a temporal gating scenario (Figure 3) can further improve SNR.

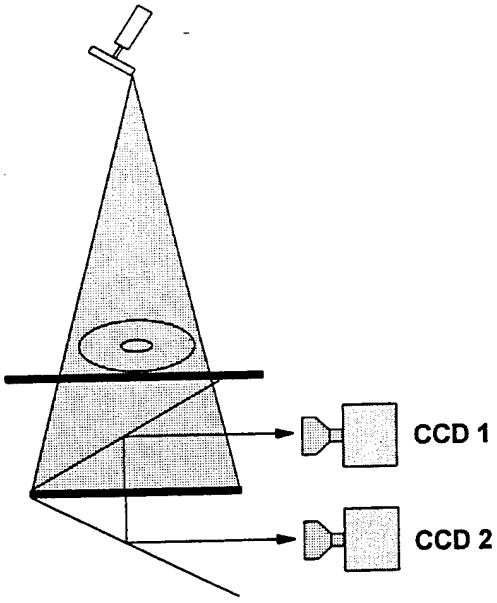

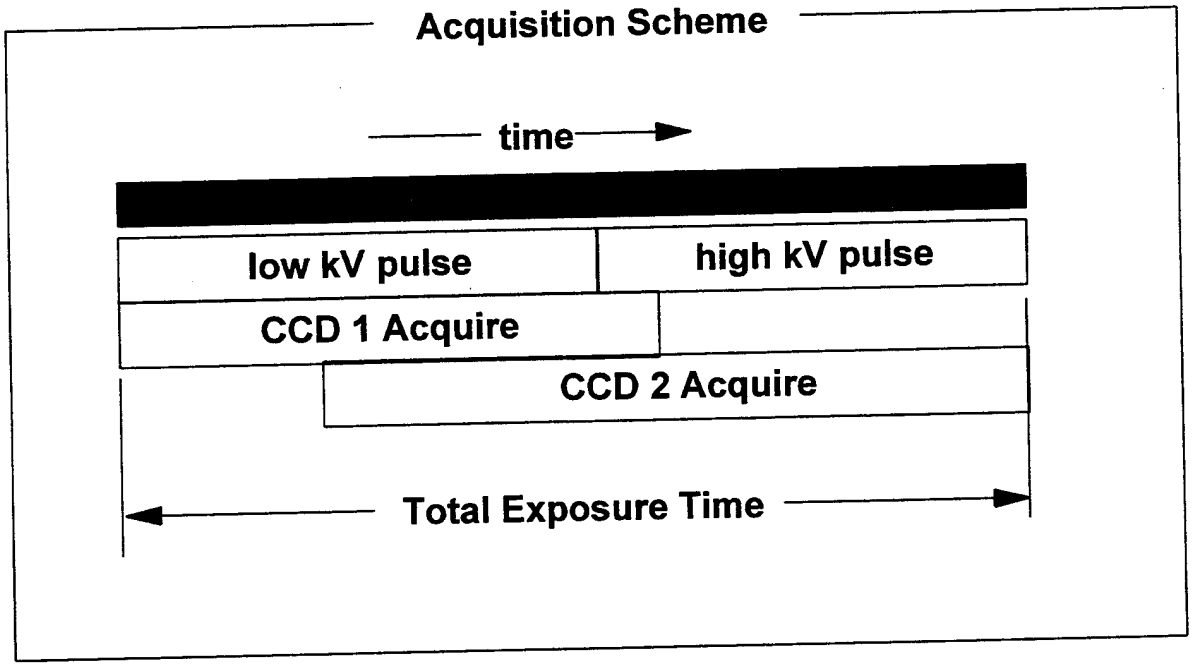

Figure3: With the installation of our new constant potential generator, we can now rapidly (1-2 ms) switch kV. This will allow the ability to improve the SNR in the dual energy subtracted images. Because the CCD cameras can be controlled independently, they can be switched on & off in a timing sequence as shown above. The transition times for each event are currently being optimized using computer simulation.

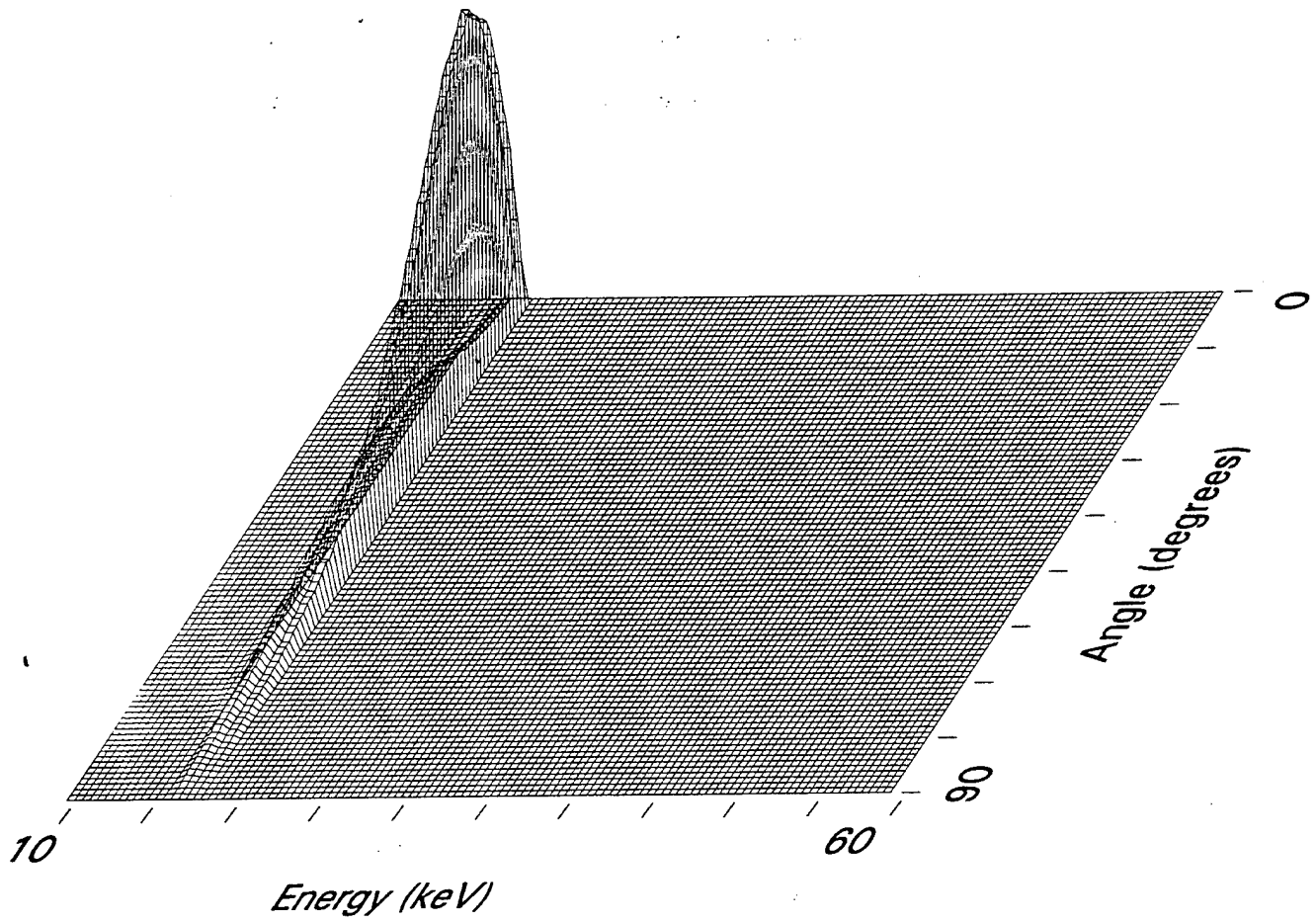

Figure 4: This is a plot of the spectral and angular distribution from a 3 cm thick breast with a 15 keV monoenergetic beam incident upon it. This data was generated using Monte Carlo simulations with 100 million input photons. Polyenergetic spectral results can be computed by combining the monoenergetic results with appropriate spectral weighting. These data are used to calculate scatter rejection (grid) efficacy as well as detector efficiency.

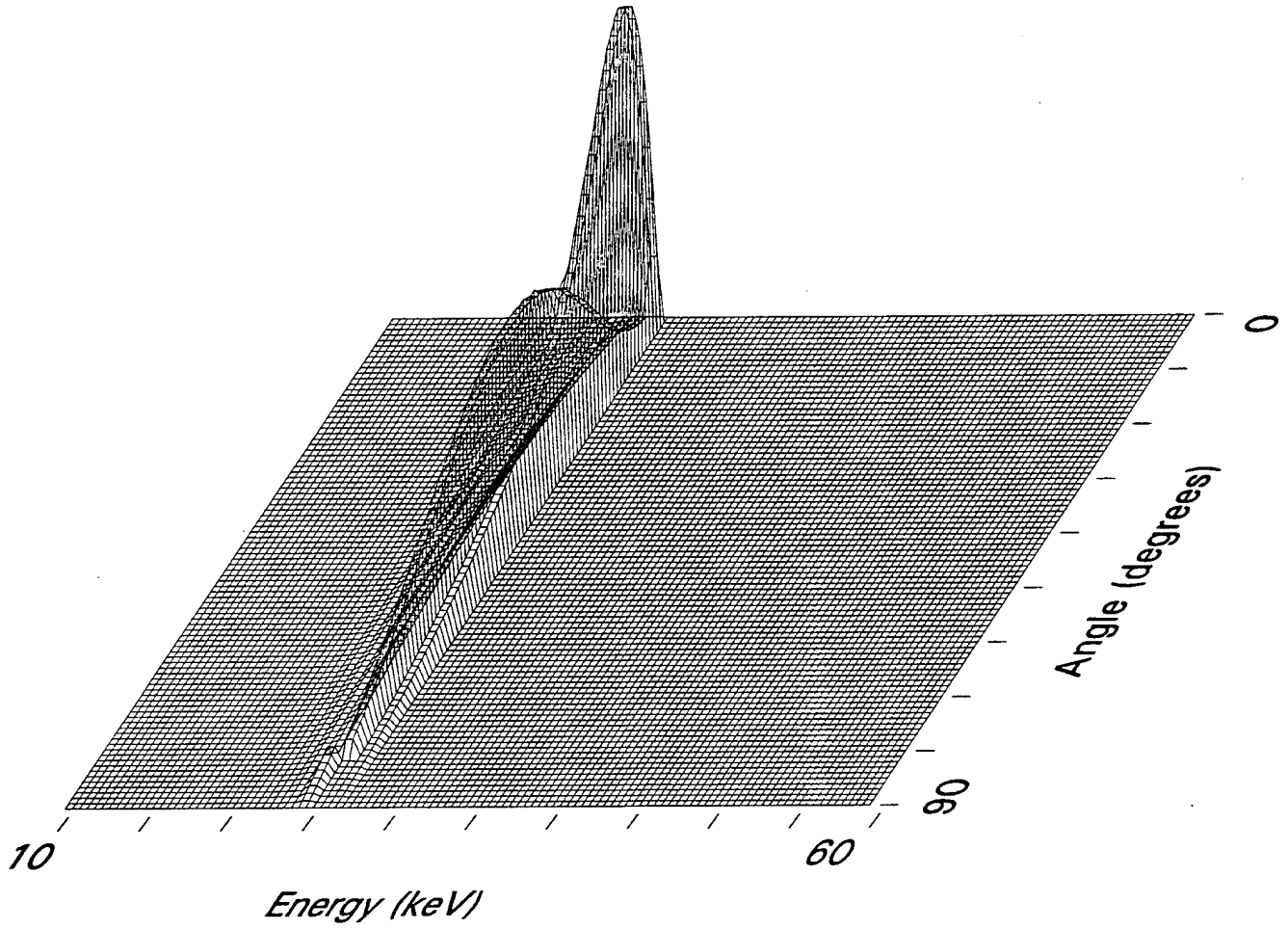

Figure 5: This is a plot of the spectral and angular distribution from a 5 cm thick breast with a 25 keV monoenergetic beam incident upon it. This data was generated using Monte Carlo simulations with 100 million input photons. Polyenergetic spectral results can be computed by combining the monoenergetic results with appropriate spectral weighting. These data are used to calculate scatter rejection (grid) efficacy as well as detector efficiency.

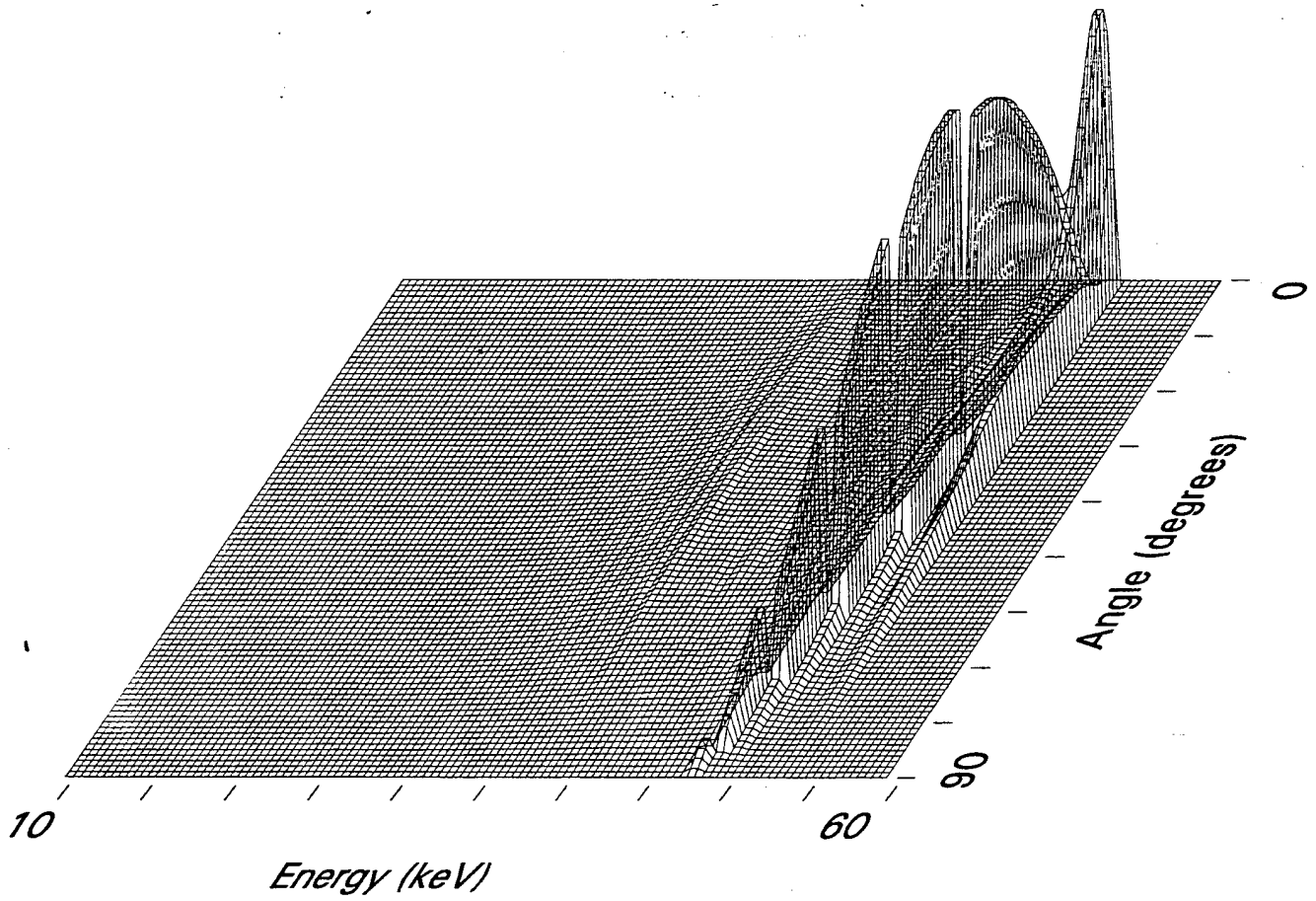

Figure 6: This is a plot of the spectral and angular distribution from a 8 cm thick breast with a 55 keV monoenergetic beam incident upon it. This data was generated using Monte Carlo simulations with 100 million input photons. Polyenergetic spectral results can be computed by combining the monoenergetic results with appropriate spectral weighting. These data are used to calculate scatter rejection (grid) efficacy as well as detector efficiency.

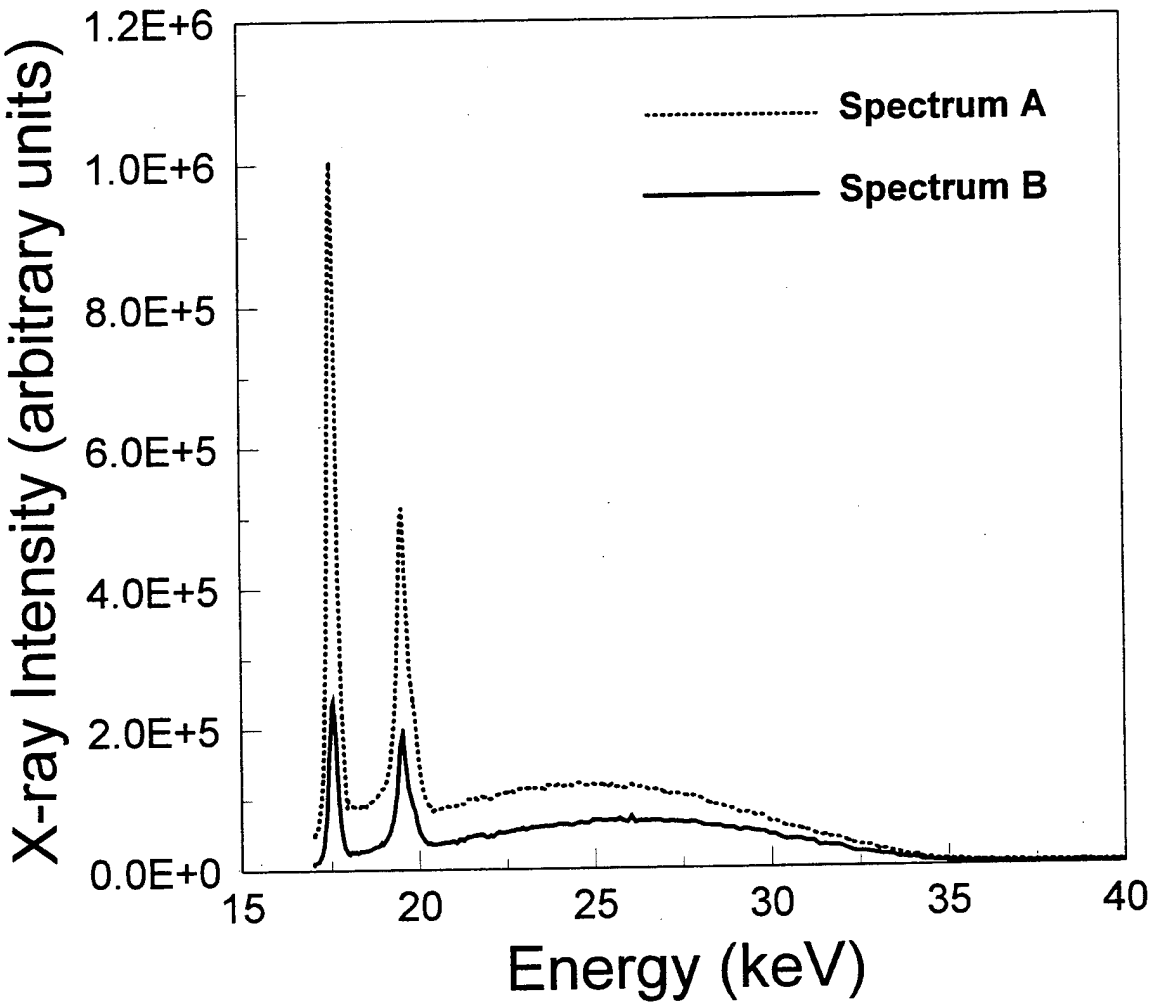

Figure 7: X-ray spectra measured in our laboratory using the Delattes spectrometer. This molybdenum anode spectrum was generated at 35 kV on a Senograph 500T mammography unit. Spectrum A was attenuated with a glass microscope slide to reduce the intensity at low energies. Spectrum B was identical to Spectrum A except that 1.0 mm of Aluminum was added to the beam.

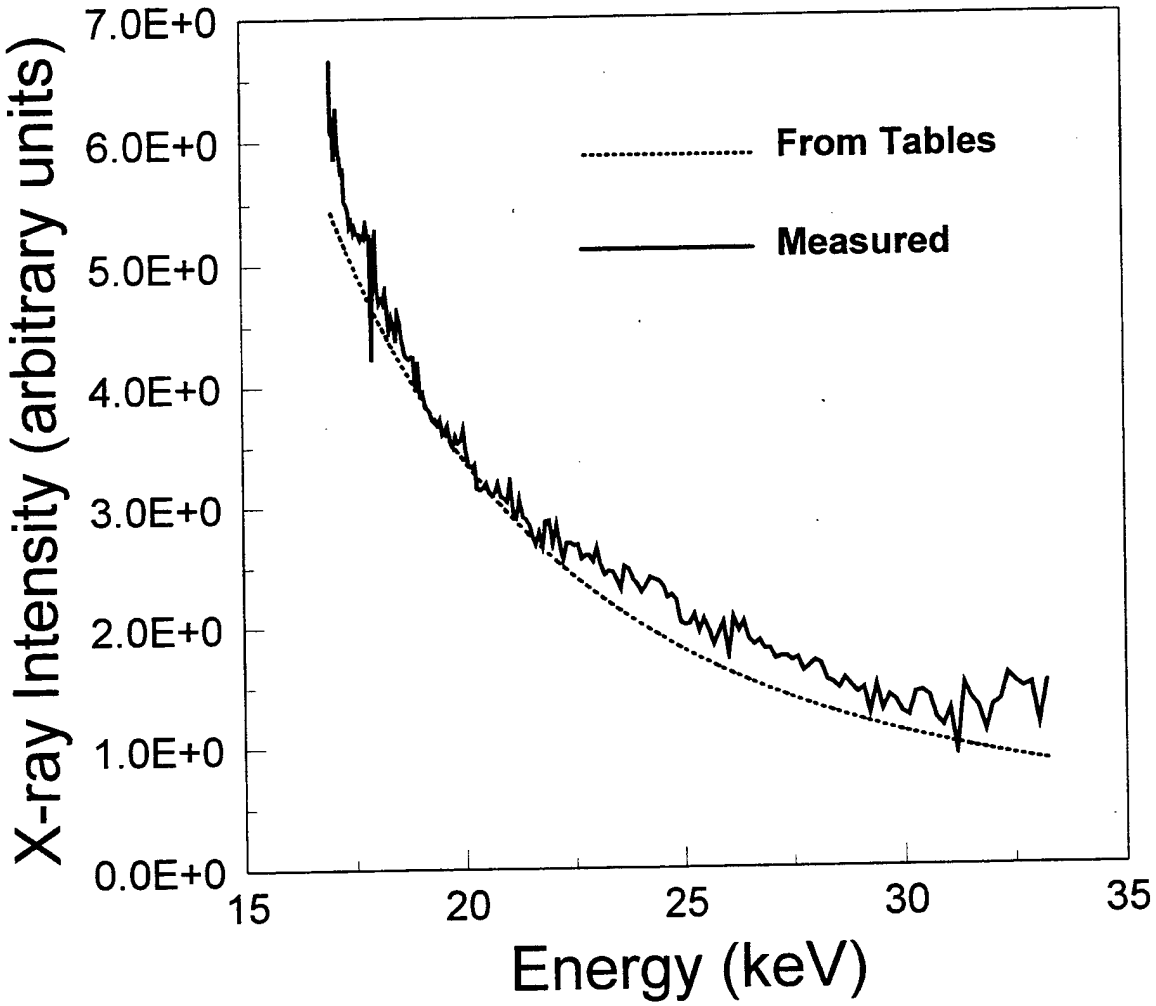

Figure 8: Attenuation data for a 1.0 mm sheet of aluminum. The dashed line is the mass attenuation coefficient for aluminum from the data tabels of McMasters. The solid line corresponds to the attenuation measured in our laboratory. These preliminary data are shown only to illustrate that attenuation measurements can be made using the Deslatte spectrometer. Inaccuracies between the two curves can be attributed to impure aluminum, inaccurate energy calibration, or fluxuation in the x-ray tube output.

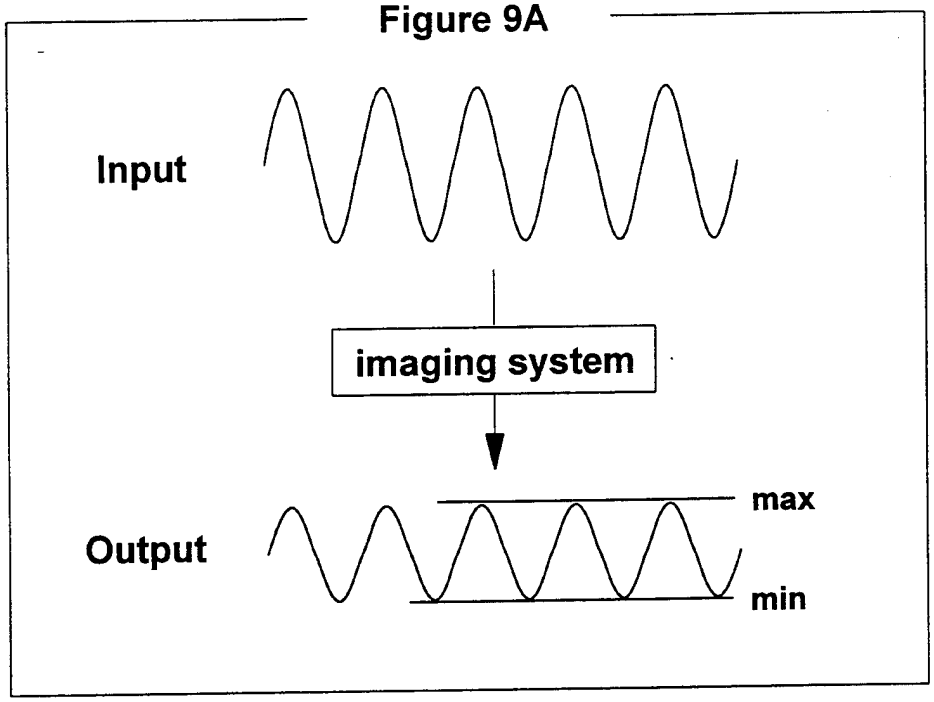

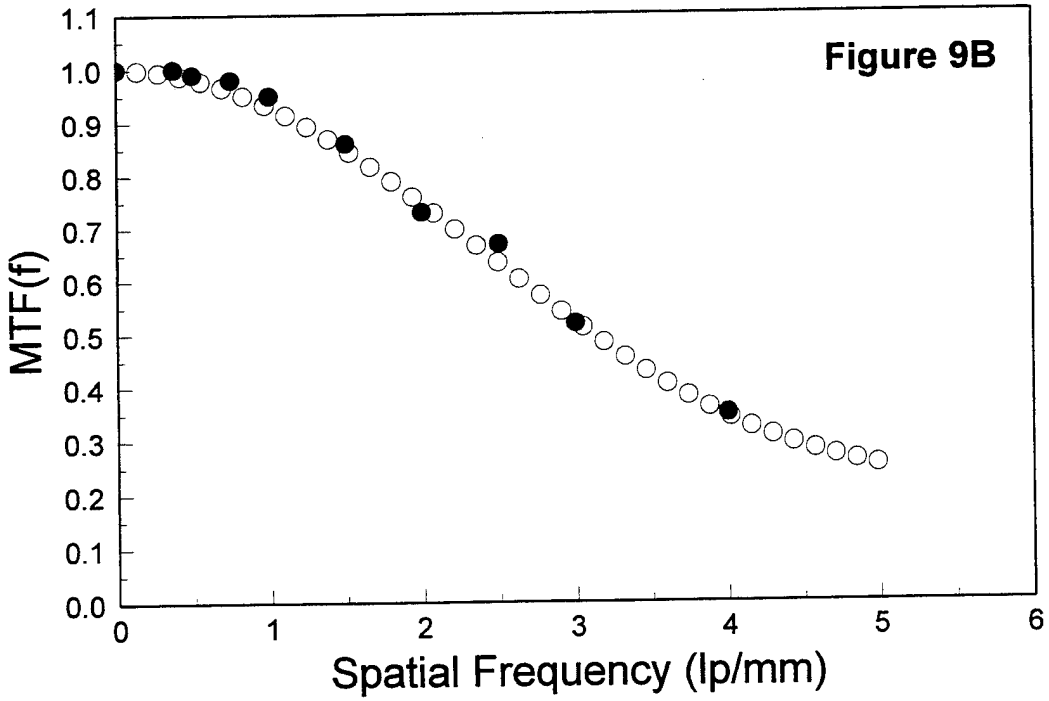

Figure 9: (A) A diagram showing the relationship between the input signal and the signal after it has been imaged by the imaging system. The modulation is calculated from the max and min signals. (B) A comparison of calculation techniques. The open circles show the MTF calculated by calculating the Fourier transform of the line spread function. The closed circles show the MTF as calculated directly from the min and the max values, using a sine wave pattern as input. The MTFs correspond to the CCD camera and optics.

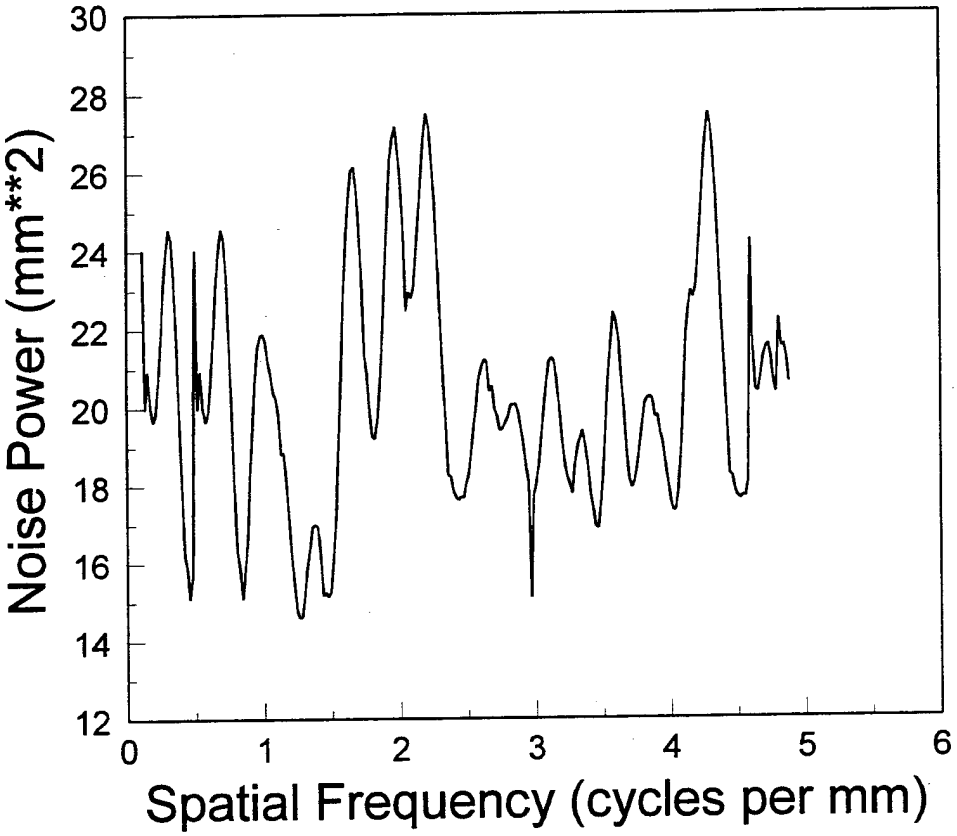

Figure 10: The Noise Power Spectrum (NPS) of the optical - CCD camera imaging system in our laboratory. We are presently making detailed NPS and DQE(f) measurements as a function of several important imaging parameters, including demagnification factor, F-stop setting, and the wavelength of the light emitted by the screen (545 and 624 nm).

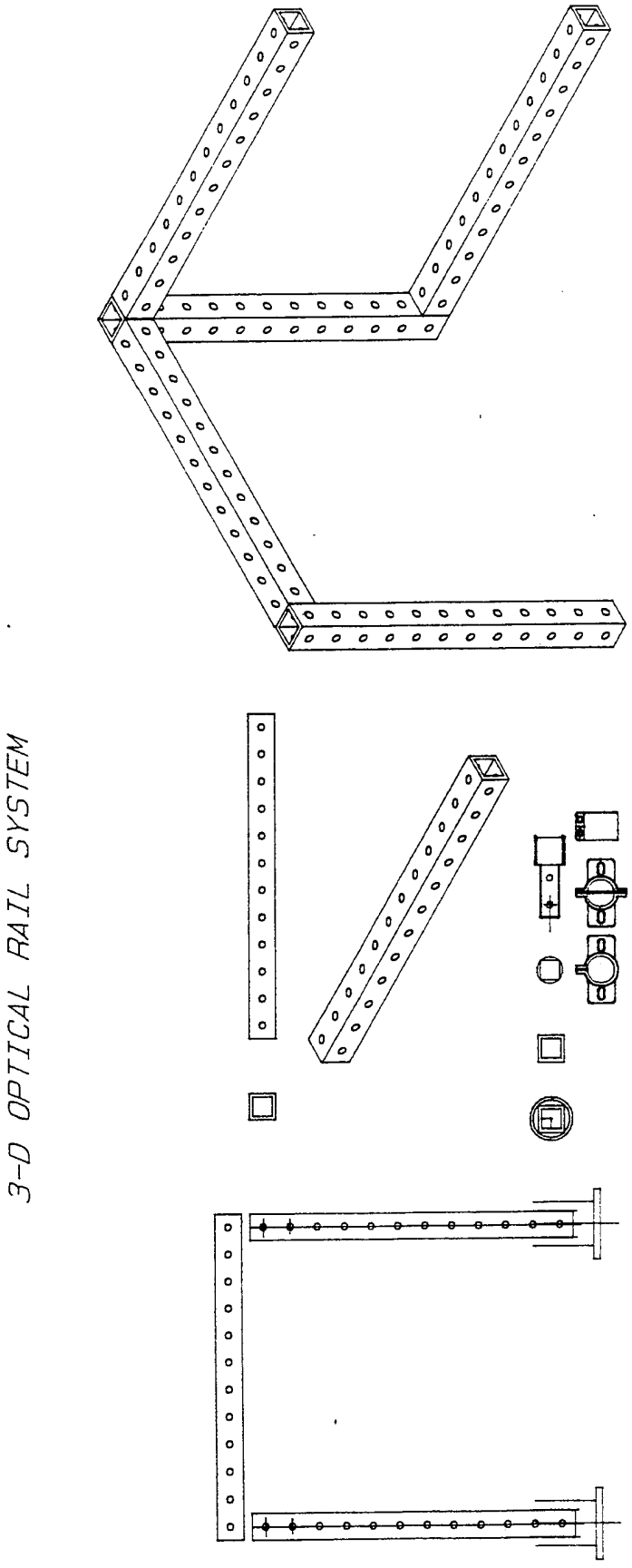

Figure 11: An engineering diagram of the optical rail system that we have designed for flexible construction of the dual energy mammographysystem.

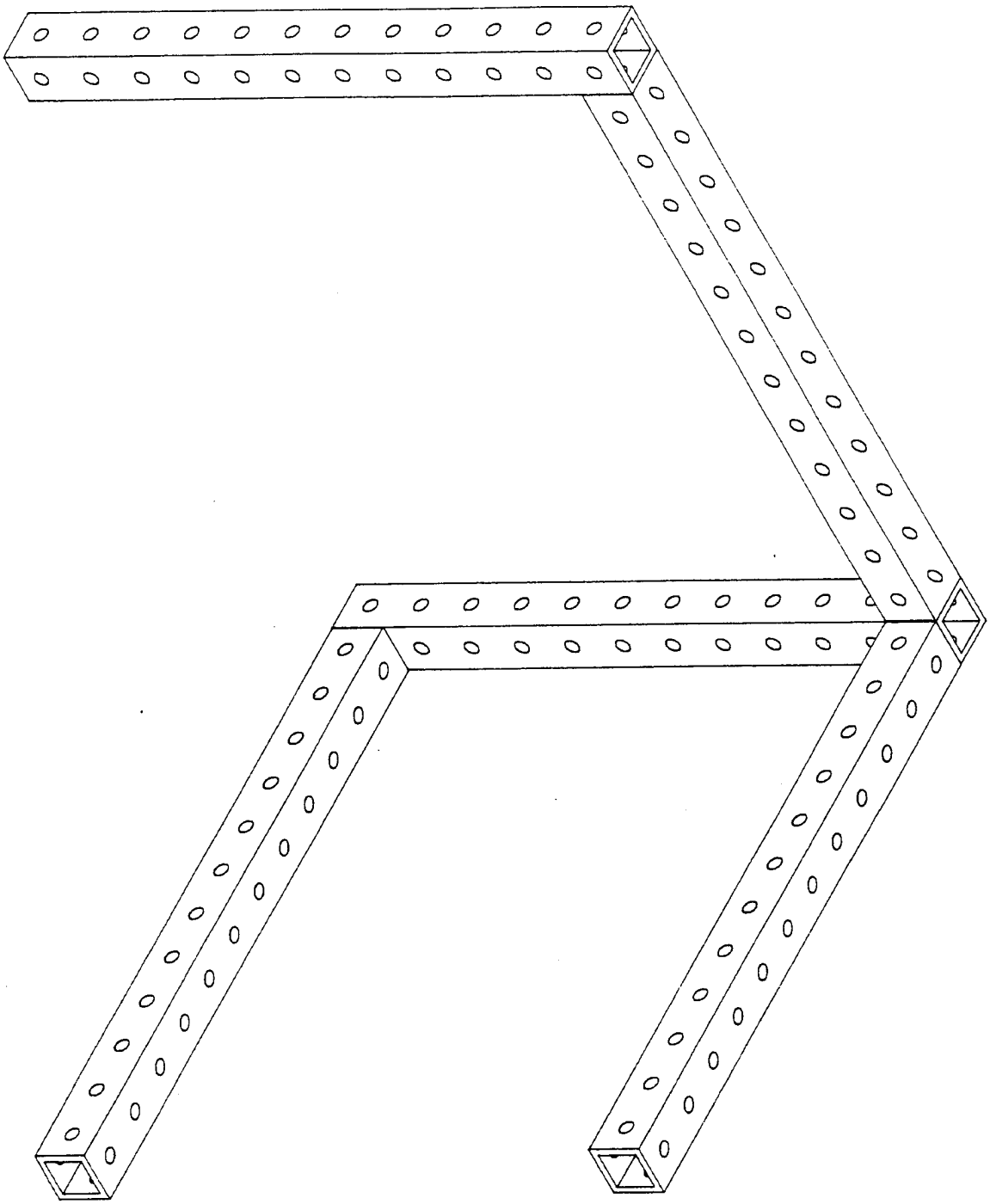

Figure 12: A blow up of the strut assembly which is the principle behind the mechanical design of the system. Struts are currently being cut to length, drilled out on 1" center, and anodized. Strut lengths include 12", 24", 36", 48" and several 96" struts. The hole spacing on the struts is compatible with the optical table, which serves as the base for the entire system. Cameras, lenses, and micropositioning equipment can be easily mounted to the strut assembly.

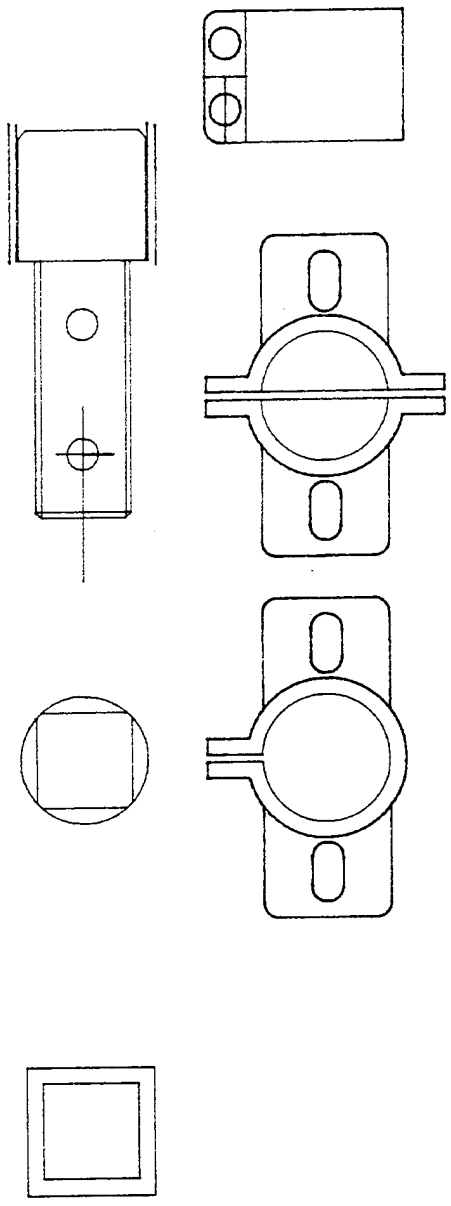

Figure 13: An engineering diagram of the coupling flanges used to connect the struts (shown in Figure 12). This type of flange will be used to position struts where the rotation angle of the suspended strut is important. Other, L-shaped flanges are being manufactured for more basic connections.